Journal of Science and Transport Technology
Journal homepage: https://jstt.vn/index.php/en

An analytical approach for nonlinear thermal buckling and postbuckling behavior of functionally graded graphene platelet-reinforced composite conical shells

Kieu Quang Thai[1], Le Ngoc Ly[2,*], Do Thi Kieu My[3]
[1]Graduate University of Science and Technology, Vietnam Academy of Science and Technology, Hanoi, Vietnam
[2]Mechanics of Advanced Materials and Structures, University of Transport Technology, Hanoi, Vietnam
[3]Institute for Building Materials and Construction Protection, Institute of Transport Science and Technology, Hanoi, Vietnam

Article info
Type of article:
Original research paper

DOI:
https://doi.org/10.58845/jstt.utt.2026.en.6.1.199-214

***Corresponding author:**
Email address:
lyln@utt.edu.vn

Received: 10/10/2025
Received in Revised Form: 10/12/2025
Accepted: 20/12/2025

Abstract: This study presents an analytical investigation into the nonlinear thermal buckling behavior of functionally graded graphene platelet-reinforced composite (FG-GPLRC) conical shells resting on a nonlinear elastic foundation. The formulation is developed based on Donnell shell theory in conjunction with von Kármán geometric nonlinearity. The nonlinear foundation is characterized by three stiffness parameters that capture both hardening and softening behaviors, corresponding to positive and negative nonlinear parameters, respectively. Employing the Ritz energy method, thermal load–deflection relationships are derived to analyze both the critical buckling temperature and the postbuckling response of the structure. The influence of key parameters, including the stiffness of the elastic medium, graphene platelet (GPL) mass fraction, material gradation profiles, and geometric configurations, on the nonlinear thermal buckling performance is thoroughly examined through numerical simulations.

Keywords: Nonlinear stability, FG-GPLRC, Donnell shell theory, Nonlinear elastic medium, Ritz energy method, Conical shell.

1. Introduction

Owing to their distinctive geometrical configuration, conical shells and panels serve as key load-bearing elements in numerous engineering applications. These structural forms are particularly prominent in the aerospace and marine sectors, where they are commonly employed in components such as ship hulls, aircraft fuselages, and other critical structure systems. Consequently, the static and dynamic behaviors of conical shells and panels, particularly issues related to stability and vibration, have been extensively investigated in the literature. An analytical method was presented by Lu and Chang [1, 2] to examine the thermal buckling and postbuckling responses of conical shells with simply supported edges and isotropic material properties, where their findings were validated against experimental data. Tani [3] explored the dynamic instability of such shells subjected to

periodic axial forces, initially neglecting and later including [4] bending deformations, applying Donnell shell theory combined with a finite difference scheme. He [5, 6] further assessed the influence of axisymmetric deflection imperfections and significant prebuckling deflections on thermal buckling behavior under uniform temperature rise [5] and combined thermal and pressure loads [6]. The vibration behavior of twisted isotropic conical shells was investigated using the Rayleigh–Ritz procedure with tapered thickness [7] and for rotating and open shells [8]. The behavior of laminated cross-ply truncated conical shells was studied by Xu et al. [9] and Patel et al. [10], utilizing shear deformation theories; the former applied the Galerkin and harmonic balance methods for free vibration analysis, while the latter adopted a semi-analytical finite element model to examine thermal nonlinear buckling phenomena. Additional investigations into the free vibration behavior of isotropic conical panels were conducted using the generalized differential quadrature (GDQ) method by Lam et al. [11] and with the mesh-free kp-Ritz technique by Zhao et al. [12]. Moreover, by applying the Ritz energy method, Paczos and Zielnica [13] evaluated the elastic–plastic stability of bilayer conical shell panels subjected to compressive and pressure loading with simple support conditions. The joined spherical-conical-cylindrical shells with multiple annular plates were mentioned by Huang et al. [14] in vibration response problems using the FSDT, spectro-geometric method, and Ritz method.

Given the widespread application of functionally graded material (FGM) structures in advanced technologies, the buckling and vibration behavior of FGM plate and shell structures have garnered considerable attention in recent research. Among the prominent studies to investigate the effects of various boundary conditions, Sofiyev [15, 16] presented the analytical approach for the linear buckling of FGM conical shells. In subsequent works, the same author [17, 18] explored the nonlinear buckling behavior of these shells under axial compression, including the effects of Winkler–Pasternak elastic foundations. His linear analyses are typically based on modified Donnell-type equations solved via the Galerkin method to derive closed-form solutions for bifurcation-type buckling loads and natural frequencies, while the nonlinear studies employ large-deflection theories incorporating von Kármán–Donnell-type geometric nonlinearity. Further contributions include Naj et al. [19], who analyzed thermal and mechanical instabilities using first-order Love–Kirchhoff shell theory coupled with Sanders' nonlinear kinematic equations. Bich et al. [20] derived linearized stability equations based on classical shell theory to study the mechanical buckling of FGM conical panels, applying the Galerkin method for explicit buckling load solutions. Malekzadeh and Heydarpour [21] investigated the free vibration behavior of rotating truncated FGM conical shells, considering the combined effects of geometric and material parameters as well as centrifugal and Coriolis forces, utilizing first-order shear deformation theory. It is important to note that these aforementioned studies primarily focus on unstiffened structures. However, in practical applications, shell elements—particularly conical ones—are often reinforced with stiffening systems to increase load-bearing capacity with minimal additional weight. Recognizing this, Crenwelge and Muster [22] adopted an energy-based method to determine the natural frequencies of ring-stiffened and combined ring-and-stringer-stiffened conical shells under simple support conditions. Mustaffa and Ali [23] employed structural symmetry techniques to study the free vibration characteristics of both cylindrical and conical stiffened shells. Additionally, Tornabene [24] and Tornabene et al. [25] presented comprehensive vibration analyses of FGM conical, cylindrical, and annular shell structures using a four-parameter power-law distribution, all within the framework of first-order shear deformation theory.

In recent years, nanocomposite materials, particularly those reinforced with carbon-based nanofillers such as carbon nanotubes (CNTs) and graphene platelets (GPLs), have emerged as promising candidates for enhancing the mechanical and thermal performance of advanced composite structures. Using the discrete singular convolution method, Mirzaei and Kiani [26] investigated the thermal buckling behavior of carbon nanotube-reinforced nanocomposite conical shells subjected to uniform temperature rise. In related studies, Ansari et al. [27, 28] determined the critical axial buckling loads of functionally graded carbon nanotube-reinforced composite (FG-CNTRC) truncated conical shells and panels. Hosseini and Talebitooti [29] further contributed by analyzing the mechanical buckling of FG-CNTRC conical shells using the GDQ method, considering the shear deformation effects. Extending the scope to functionally graded graphene platelet-reinforced composite (FG-GPLRC), the nonlinear buckling of FG-GPLRC cylindrical shells was studied with orthogonal stiffeners and Ritz energy method [30], spiral stiffeners and Galerkin method [31]. Kiani [32], Ansari et al. [33], and Mahani et al. [34] carried out analyses on the buckling and postbuckling behavior of FG-GPLRC conical shells under various loading conditions, including external pressure, axial compression, and thermal environments. Yang et al. [35] explored the nonlinear dynamic response of FG-GPLRC sandwich conical shells with variable thickness, incorporating internal resonance effects through the use of first-order shear deformation theory (FSDT) and the Galerkin method. Heydarpour [36] conducted thermoelastic analyses of rotating FG-GPLRC conical shells under thermal shock conditions, applying a hybrid approach based on transformed differential quadrature and NURBS techniques. Additionally, Saboori and Ghadiri [37] examined the nonlinear vibration characteristics of porous FG-GPLRC conical shells, accounting for both internal and external resonance phenomena using FSDT in conjunction with perturbation methods. On the nano scale, the flexoelectric effect was investigated in the buckling problems of variable thickness cracked nanoplates [38] using phase-field theory.

To the best of the authors' knowledge, the nonlinear thermal buckling behavior of FG-GPLRC conical shells embedded in a nonlinear elastic foundation has not yet been addressed in existing literature. Motivated by this gap, the present work proposes an analytical framework to study the thermal buckling and postbuckling responses of such shells, employing Donnell-type shell theory in conjunction with von Kármán geometric nonlinearity. Fundamental relations involving strain–displacement, stress–strain behavior, and internal forces and moments are systematically derived. The total potential energy associated with both buckling and postbuckling states is formulated, and the Ritz energy method is subsequently applied to obtain the corresponding nonlinear load–deflection equations. A comprehensive numerical investigation is conducted to assess the influence of key geometric dimensions, material gradation patterns, and foundation stiffness parameters on the thermal stability characteristics of FG-GPLRC conical shells, thereby validating the effectiveness and applicability of the proposed approach.

2. Geometrical and material properties of FG-GPLRC conical shells

Consider an FG-GPLRC conical shell surrounded by a nonlinear elastic foundation. The geometry of the shell is shown in Fig. 1, where h is the shell thickness, α is semi-top angle, L is the length and R_1 and R_2 are small and large base radii. The FG-GPLRC conical shell is placed in the curvilinear coordinate system (x,θ,z) with the origin placed at the mid-plane. Additionally, x_0 is defined to be the distance from the top to the small

base, and u, v and w respectively denote the displacements of a point in the mid-plane in the directions x, θ and z.

The mass fraction of GPL is designed in three distribution patterns, including UD, FG-X, and FG-O. The extended Halpin-Tsai model can be used to predict the effective elastic modulus, as [30-33]

$$E(z) = \frac{3}{8}\frac{1+\zeta_1\delta_1 V_{GPL}(z)}{1-\delta_1 V_{GPL}(z)}E_m + \frac{5}{8}\frac{1+\zeta_2\delta_2 V_{GPL}(z)}{1-\delta_2 V_{GPL}(z)}E_{m,} \quad (1)$$

where

$$\delta_1 = \frac{(E_{GPL}/E_m)-1}{(E_{GPL}/E_m)+\zeta_1},\ \delta_2 = \frac{(E_{GPL}/E_m)-1}{(E_{GPL}/E_m)+\zeta_2}, \quad (2)$$
$$\zeta_1 = 2(a_{GPL}/t_{GPL}),\ \zeta_2 = 2(b_{GPL}/t_{GPL}),$$

with E_m and E_{GPL} are the elastic moduli of the matrix and GPL, respectively; a_{GPL}, b_{GPL}, t_{GPL} are the denotes of the length, width, and thickness of GPL, respectively, and the volume fraction of the GPL is presented by V_{GPL}, as

$$V_{GPL}(z) = \frac{\overline{W}_{GPL}}{\overline{W}_{GPL} + (\rho_{GPL}/\rho_m)(1-\overline{W}_{GPL})}, \quad (3)$$

where $V_m + V_{GPL} = 1$; the densities of the matrix and the GPL are ρ_m and ρ_{GPL}, respectively, $\overline{W}_{GPL}$ is the mass fraction of GPL along the shell thickness (Fig. 2), designed as

$$\overline{W}_{GPL}(z) = \begin{cases} W_{GPL} & \text{for } \frac{-h}{2} \le z \le \frac{h}{2} \quad \text{UD,} \\ 4\frac{|z|}{h}W_{GPL} & \text{for } \frac{-h}{2} \le z \le \frac{h}{2} \quad \text{FG-X,} \\ 2\left(1-\frac{2|z|}{h}\right)W_{GPL} & \text{for } \frac{-h}{2} \le z \le \frac{h}{2} \quad \text{FG-O,} \end{cases} \quad (4)$$

where the total GPL mass fraction is denoted by W_{GPL}.

According to the mixture rule, the Poisson ratio and thermal expansion coefficient can be estimated by

$$\nu(z) = \nu_m(1-V_{GPL}) + \nu_{GPL}V_{GPL},$$
$$\alpha(z) = \alpha_m(1-V_{GPL}) + \alpha_{GPL}V_{GPL}. \quad (5)$$

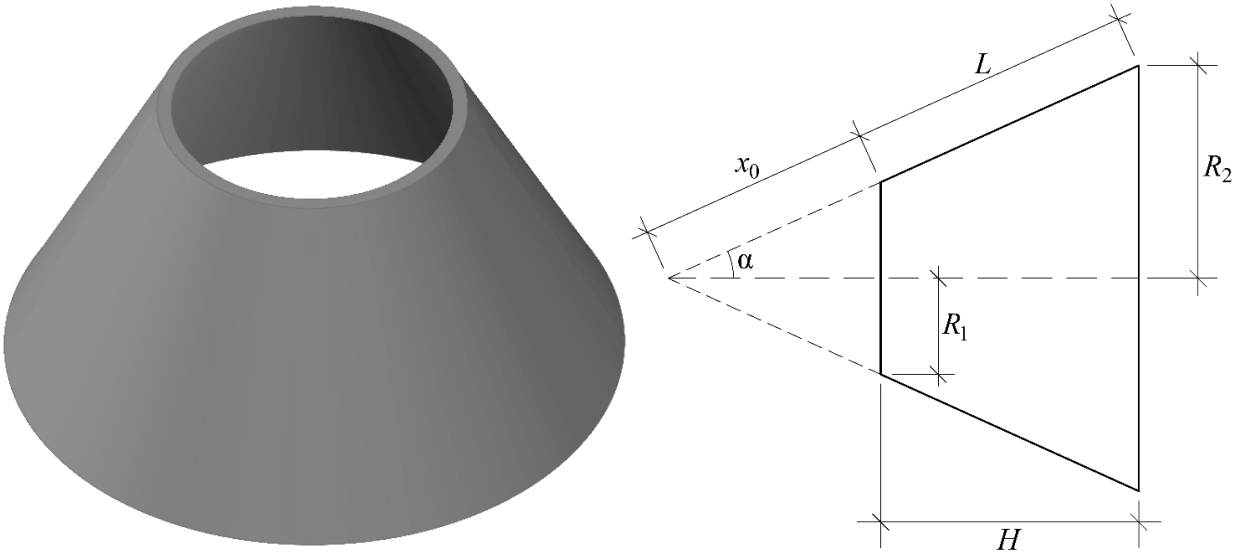

Fig. 1. Configurations and geometrical parameters of FG-GPLRC conical shells

Fig. 2. GPL distribution patterns of FG-GPLRC

3. Theoretical formulations

The strains of the conical shells according to the Donnel shell theory with nonlinear large deflection theory at a distance of z from the mid-plane can be written by [16]

$$\varepsilon_x = z\kappa_x + \varepsilon_{0x}, \varepsilon_\theta = z\kappa_\theta + \varepsilon_{0\theta}, \gamma_{x\theta} = z\kappa_{x\theta} + \gamma_{0x\theta}, \quad (6)$$

where (7)

$$\varepsilon_{0x} = \frac{\partial}{\partial x}u(x,\theta) + \frac{1}{2}\left(\frac{\partial}{\partial x}w(x,\theta)\right)^2,$$

$$\varepsilon_{0\theta} = \frac{\frac{\partial}{\partial\theta}v(x,\theta)}{x\sin(\alpha)} + \frac{u(x,\theta)}{x} + \frac{w(x,\theta)\cot(\alpha)}{x} + \frac{1}{2}\frac{\left(\frac{\partial}{\partial\theta}w(x,\theta)\right)^2}{x^2\left(\sin(\alpha)\right)^2},$$

$$\gamma_{0x\theta} = \frac{\frac{\partial}{\partial\theta}u(x,\theta)}{x\sin(\alpha)} - \frac{v(x,\theta)}{x} + \frac{\partial}{\partial x}v(x,\theta) + \frac{\left(\frac{\partial}{\partial x}w(x,\theta)\right)\frac{\partial}{\partial\theta}w(x,\theta)}{x\sin(\alpha)}$$

$$\kappa_x = -\frac{\partial^2}{\partial x^2}w(x,\theta),$$

$$\kappa_\theta = -\frac{\frac{\partial^2}{\partial\theta^2}w(x,\theta)}{x^2\left(\sin(\alpha)\right)^2} - \frac{\frac{\partial}{\partial x}w(x,\theta)}{x}, \quad (8)$$

$$\kappa_{x\theta} = -2\frac{\frac{\partial^2}{\partial x\partial\theta}w(x,\theta)}{x\sin(\alpha)} + 2\frac{\frac{\partial}{\partial\theta}w(x,\theta)}{x^2\sin(\alpha)}.$$

Hooke's law is used for the FG-GPLRC conical shells, considering the thermal strains, as

$$\sigma_x = Q_{11}(\varepsilon_x - \Delta T\alpha_1) + Q_{12}(\varepsilon_\theta - \Delta T\alpha_2),$$
$$\sigma_\theta = Q_{12}(\varepsilon_x - \Delta T\alpha_1) + Q_{22}(\varepsilon_\theta - \Delta T\alpha_2), \quad (9)$$
$$\tau_{x\theta} = Q_{66}\gamma_{x\theta},$$

where ΔT is the uniformly distributed thermal load, and the reduced stiffnesses are presented as

$$Q_{11} = Q_{22} = \frac{E^2(z)}{1-\nu^2(z)}, Q_{12} = \frac{\nu(z)E^2(z)}{1-\nu^2(z)}, \quad Q_{66} = \frac{E(z)}{2\left[1+\nu(z)\right]}. \quad (10)$$

The internal forces and moments of the FG-GPLRC conical shells are determined by integrating Hooke's law, obtained as

$$N_x = A_{11}\varepsilon_{0x} + A_{12}\varepsilon_{0\theta} + B_{11}\kappa_x + B_{12}\kappa_\theta - \Phi_{1x}\Delta T,$$
$$N_\theta = A_{12}\varepsilon_{0x} + A_{22}\varepsilon_{0\theta} + B_{12}\kappa_x + B_{22}\kappa_\theta - \Phi_{1\theta}\Delta T, \quad (11)$$
$$N_{x\theta} = A_{66}\gamma_{0x\theta} + B_{66}\kappa_{x\theta},$$

$$M_x = B_{11}\varepsilon_{0x} + B_{12}\varepsilon_{0\theta} + D_{11}\kappa_x + D_{12}\kappa_\theta - \Phi_{2x}\Delta T,$$
$$M_\theta = B_{12}\varepsilon_{0x} + B_{22}\varepsilon_{0\theta} + D_{12}\kappa_x + D_{22}\kappa_\theta - \Phi_{2\theta}\Delta T, \quad (12)$$
$$M_{x\theta} = B_{66}\gamma_{0x\theta} + D_{66}\kappa_{x\theta},$$

where the stiffnesses are determined by

$$\left(A_{ij}, B_{ij}, D_{ij}\right) = \int_{-h/2}^{h/2} Q_{ijs(k)}\left(1, z, z^2\right)dz, (i,j = 1,2,6) \quad (13)$$

The thermo-elastic strain energy of the FG-GPLRC conical shells can be calculated as

$$U_{int} = \frac{1}{2}\int_{x_0}^{x_0+L}\int_0^{2\pi}\int_{-h/2}^{h/2}\begin{pmatrix}\sigma_x(\varepsilon_x - \alpha_1\Delta T)\\ +\sigma_\theta(\varepsilon_\theta - \alpha_2\Delta T)\\ +\tau_{x\theta}\gamma_{x\theta}\end{pmatrix}\times x\sin(\alpha)\,dz\,d\theta\,dx. \quad (14)$$

The work done by the shell-foundation interaction, presented as

$$U_{ext} = \int_{x_0}^{x_0+L}\int_0^{2\pi}\left[\begin{pmatrix}K_1 w + \\ K_2\left(w_{,xx} + \frac{w_{,x}}{x} + \frac{w_{,\theta\theta}}{x^2\left(\sin(\alpha)\right)^2}\right)\end{pmatrix}\times w(x,\theta).x.\sin(\alpha)\right]d\theta\,dx + \frac{1}{4}\int_{x_0}^{x_0+L}\int_0^{2\pi}\left(K_3.\left(w(x,\theta)\right)^4.x.\sin(\alpha)\right)d\theta\,dx, \quad (15)$$

where K_1 (N/m^3), K_2 (N/m), and K_3 (N/m^5) are the stiffnesses of Winkler, Pasternak, and nonlinear models, respectively.

In this paper, the nonlinear thermal buckling behavior of FG-GPLRC conical shells is considered with the assumption of simply supported and immovable at both ends. The corresponding boundary conditions are expressed as

$$u = v = u = 0, M_x = 0 \text{ at } x = x_0, x = x_0 + L. \quad (16)$$

The approximate solutions of the displacements and deflection chosen to satisfy the boundary condition (16), and the closed circumferential condition of shells are proposed by

$$u = U\sin\left(\frac{2m\pi(x-x_0)}{L}\right)\sin(n\theta),$$

$$v = V\sin\left(\frac{m\pi(x-x_0)}{L}\right)\sin(2n\theta), \quad (17)$$

$$w = W\sin\left(\frac{m\pi(x-x_0)}{L}\right)\sin(n\theta).$$

The total potential energy is obtained as

$$A = U_{int} - U_{ext}. \quad (18)$$

By using Eqs. (9, 11,12, 14, 15, 17), the total energy expression in Eq. (18) can be rewritten with respect to the displacements u and w. Then, the approximate displacements and deflection in Eq. (18) are substituted into the resulting total potential energy. The Ritz energy method can be applied, as

$$\frac{\partial A}{\partial U} = \frac{\partial A}{\partial V} = \frac{\partial A}{\partial W} = 0, \quad (19)$$

leads to

$$Ub_1 + Wb_2 = 0, \quad (20)$$

$$W^2 b_3 + Vb_4 = 0, \quad (21)$$

$$W^3 b_5 + VWb_6 + Wb_7\Delta T + Ub_8 + Wb_9 = 0, \quad (22)$$

where the coefficients b_i are presented in the Appendix.

The displacement amplitudes U and V can be obtained from Eqs. (20) and (21), as

$$U = -\frac{Wb_2}{b_1}, \quad (23)$$

$$V = -\frac{W^2 b_3}{b_4}. \quad (24)$$

Substituting displacement amplitudes U and V from Eqs. (23) and (24) into Eq. (22), the thermal postbuckling expression can be obtained by

$$\Delta T = T_1 W^2 + T_2, \quad (25)$$

where

$$T_1 = \frac{b_3 b_6 - b_4 b_5}{b_4 b_7}, T_2 = \frac{-b_1 b_4 b_9 + b_2 b_4 b_8}{b_4 b_1 b_7}. \quad (26)$$

The bifurcation thermal buckling load of shells can be determined from Eq. (25) by applying $W \to 0$, as

$$T_{bk} = T_2. \quad (27)$$

The thermal buckling load T_{bk} depends on the m and n values. By minimizing the thermal buckling load with respect to m and n, the critical thermal buckling load T_{cr} can be obtained.

4. Results and discussions

The critical thermal buckling loads for the FGM conical shells are investigated to validate the present approach in Table 1. The present results are compared with those of Sofiyev [15], who applied the modified Donnell shell theory and Galerkin method. As can be observed, good agreements are observed in these comparisons. In this paper, the temperature-independent material properties of Copper/GPL FG-GPLRC can be referred to in the previous report of Wang et al. [39]. Effects of GPL distribution patterns and semi-top angle on the critical thermal buckling load of FG-GPLRC conical shells are investigated in Table 2. The results indicate a clear dependence of the buckling performance on both the material distributions and the shell geometry. Among the three distribution types, the FG-X pattern consistently exhibits the highest critical thermal buckling loads, followed by the UD and FG-O configurations. This superior performance of FG-X can be attributed to the concentration of GPL near both the inner and outer surfaces of the shell, where the stress levels are typically more significant under thermal loading. In contrast, the FG-O distribution, which accumulates GPLs near the mid-plane, demonstrates the lowest buckling resistance, suggesting a less efficient reinforcement strategy for stability enhancement.

Furthermore, an increase in the semi-top angle generally leads to a rise in the critical buckling temperature for all distribution patterns. For instance, when the semi-top angle increases from 10° to 20°, the buckling load increases significantly across all material configurations, emphasizing the beneficial role of geometrical tuning in thermal stability optimization. In addition to these observations, it is also noteworthy that the buckling mode numbers, denoted in parentheses in Table 2, vary with both the GPL distribution and geometric parameters.

Table 1. Comparison of critical thermal buckling load T_{cr} (^{0}C) of FGM conical shells with those of Sofiyev [15] (Without foundation, $E_m = 70GPa$, $\alpha_m = 2.3\times10^{-5}K^{-1}$, $E_c = 380GPa$, $\alpha_c = 7.4\times10^{-6}K^{-1}$, $R = 0.25m$)

α	d	R/h = 100			R/h = 200		
		Sofiyev [15]	Present	%	Sofiyev [15]	Present	%
10^0	2	426	423.748	0.53	213	211.767	0.58
	3	410	411.539	0.37	205	205.358	0.17
15^0	2	451	474.427	4.94	226	237.166	4.71
	3	434	460.684	5.79	217	229.806	5.57

Table 2. Effects of GPL distribution patterns and semi-top angle α on the critical thermal buckling load T_{cr} (K) of FG-GPLRC conical shells $\left(h = 2mm,\ R_2 = 100h, H = 2R_2, K_1 = 2\times10^7\ N/m^3, K_2 = 10^5\ N/m\right)$

	FG-X	UD	FG-O
$\alpha = 10^0$	344.176 (13;1)*	327.840 (13;3)	311.883 (13;5)
$\alpha = 15^0$	384.509 (14;1)	366.260 (14;3)	348.466 (14;4)
$\alpha = 20^0$	446.670 (15;2)	425.246 (16;1)	404.190 (16;2)

* The buckling modes $(m;n)$

Table 3. Effects of R_2/h ratios on the critical thermal buckling load T_{cr} (K) of FG-GPLRC conical shells $\left(h = 2mm,\ \alpha = 10^0, H = 2R_2, K_1 = 2\times10^7\ N/m^3, K_2 = 10^5\ N/m\right)$

R_2/h	FG-X	UD	FG-O
100	344.176 (13;1)*	327.840 (13;3)	311.883 (13;5)
150	233.334 (15;6)	222.432 (16;3)	211.821 (16;5)
200	177.809 (18;3)	169.682 (18;6)	161.694 (19;3)

Table 4. Effects of foundation parameters on the critical thermal buckling load T_{cr} (K) of FG-GPLRC conical shells $\left(h = 2mm,\ R_2 = 100h, H = 2R_2, \alpha = 10^0\right)$

	FG-X	UD	FG-O
$K_1 = K_2 = 0$	332.185 (13;1)	315.896 (13;3)	299.872 (13;5)
$K_1 = 2\times10^7\ N/m^3$, $K_2 = 1\times10^5\ N/m$	344.176 (13;1)	327.840 (13;3)	311.883 (13;5)
$K_1 = 3\times10^7\ N/m^3$, $K_2 = 2\times10^5\ N/m$	356.288 (13;1)	339.901 (13;3)	324.004 (13;5)

Table 3 illustrates the effect of the geometric slenderness, represented by the radius-to-thickness ratio R_2/h, on the critical thermal buckling load for FG-GPLRC conical shells with different GPL distribution patterns. As R_2/h increases from 100 to 200, a significant reduction

in the critical buckling temperature is observed across all distribution types. This inverse relationship between R_2/h and the buckling load can be attributed to the decrease in shell stiffness associated with increasing slenderness. Specifically, as the shell becomes thinner relative to its radius, it becomes more susceptible to instability under thermal loading. This trend is consistent with a real phenomenon, where increased slenderness generally reduces the structure's capacity to resist deformation. Among the three distribution patterns, the FG-X configuration consistently outperforms the UD and FG-O counterparts at all R_2/h values, reaffirming the earlier conclusion regarding the superior reinforcement efficiency of the FG-X gradation. However, it is worth noting that the rate of degradation in buckling performance with increasing R_2/h is relatively uniform across all configurations, suggesting that material distribution has a dominant effect at lower R_2/h values, while geometric slenderness becomes the controlling factor at higher ratios. Furthermore, the accompanying mode numbers indicate shifts to higher circumferential and axial wave numbers as R_2/h increases, reflecting a transition to more complex buckling patterns in slender shells. This mode evolution underlines the increasing geometric sensitivity of the system as the shell becomes thinner, which must be carefully considered in design applications.

Table 4 investigates the influence of the elastic foundation parameters, specifically the Winkler and Pasternak stiffness coefficients, on the critical thermal buckling load of FG-GPLRC conical shells with three different GPL distribution patterns. The results clearly demonstrate that increasing the stiffness of the foundation leads to a substantial enhancement in thermal buckling resistance across all configurations. In the absence of foundation support ($K_1 = K_2 = 0$), the shells exhibit the lowest critical buckling loads. Introducing a linear elastic foundation ($K_1 = 2\times10^7$ N/m^3, $K_2 = 1\times10^5$ N/m) leads to a notable increase in the buckling load. Further increasing the foundation stiffness ($K_1 = 3\times10^7$ N/m^3, $K_2 = 2\times10^5$ N/m) amplifies this stabilizing effect. This trend highlights the crucial role of the surrounding medium in constraining the lateral and shear deformations of the shell, thereby improving its overall stability under thermal loading. It is also important to note that the buckling modes remain constant across different foundation parameters within each material configuration. This consistency suggests that while the foundation significantly increases the buckling threshold, it does not fundamentally alter the dominant buckling mechanism under thermal loads.

Table 5. Effects of mass fraction W_{GPL} on the critical thermal buckling load T_{cr} (K) of FG-GPLRC conical shells $\left(h = 2mm, \alpha = 10^0, H = 2R_2, R_2 = 100h, K_1 = 3\times10^7\,N/m^3,\ K_2 = 2\times10^5\,N/m\right)$

W_{GPL}	FG-X	UD	FG-O
0.1%	339.592 (13;2)	335.589 (13;3)	331.610 (13;3)
0.3%	348.307 (13;1)	337.532 (13;3)	326.917 (13;4)
0.5%	356.288 (13;1)	339.901 (13;3)	324.004 (13;5)

Table 5 explores the sensitivity of the critical thermal buckling load of FG-GPLRC conical shells to variations in the total mass fraction of GPL W_{GPL} for three different material distribution patterns. The mass fraction values considered range from 0.1% to 0.5%, reflecting practical reinforcement levels in advanced composite design. The results show a consistent and monotonic increase in the critical thermal buckling load as the GPL mass fraction increases, regardless of the distribution type. This enhancement is a direct consequence of the improved stiffness of the composite due to the

inclusion of highly rigid GPLs. As the mass fraction rises, the overall elastic modulus of the functionally graded composite increases, thereby elevating the shell's resistance to thermally induced instability. Additionally, minor variations in the associated buckling mode numbers indicate that increasing the GPL content slightly influences the buckling pattern, particularly for the FG-O configuration, which transitions across modes more frequently as the reinforcement level changes. This mode sensitivity could be attributed to the more uniform or mid-thickness GPL distribution, which provides less targeted stiffening. Table 6 presents the influence of shell thickness h on the critical thermal buckling load of FG-GPLRC conical shells for three distinct GPL distribution patterns. The values of thickness considered, including 1 mm, 2 mm, and 3 mm, span a practical range for thin-walled conical structures used in aerospace and mechanical applications. As expected, increasing the shell thickness leads to a substantial and nearly proportional rise in the critical thermal buckling load. This trend can be attributed to the fact that thicker shells possess greater bending stiffness and thermal resistance, which in turn enhance their capacity to withstand compressive thermal stresses without undergoing instability. Specifically, the critical load for the FG-X shell increases from approximately 190.29K at h=1 mm to over 506.25K at h=3 mm, representing a performance gain of more than 160%. Interestingly, changes in the associated buckling mode numbers across thicknesses indicate that not only does the thermal stability improve, but the shell may also transition to lower-order buckling modes as it becomes stiffer. This shift suggests a qualitative change in the buckling behavior that must be accounted for in design and analysis.

Table 6. Effects of shell thickness h on the critical thermal buckling loads T_{cr} (K) of FG-GPLRC conical shells $\left(\alpha = 10^0, H = 2R_2, R_2 = 0.2\text{m}, W_{GPL} = 0.5\%, h = 2\text{mm}, K_1 = 2\times10^7\ \text{N/m}^3,\ K_2 = 10^5\ \text{N/m}\right)$

h	FG-X	UD	FG-O
1mm	190.289 (18;3)	182.094 (18;6)	174.150 (19;3)
2mm	344.176 (13;1)	327.840 (13;3)	311.883 (13;5)
3mm	506.246 (10;4)	482.012 (10;5)	457.650 (11;2)

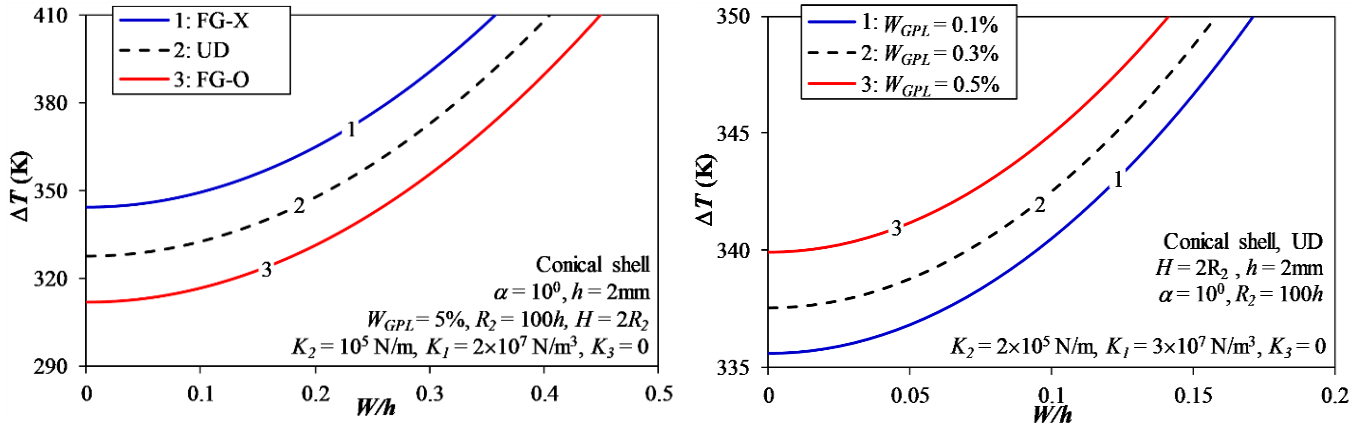

(a) (b)

Fig. 3. Effects of GPL distribution patterns and GPL mass fraction on the thermal postbuckling of FG-GPLRC conical shells

Fig. 3 illustrates the thermal postbuckling response of FG-GPLRC conical shells, focusing on the influence of GPL distribution patterns and mass fraction levels. The plots provide insight into the

nonlinear load–deflection characteristics beyond the critical buckling point, which is essential for assessing structural safety under increasing thermal environments. In Fig. 3(a), the comparison among the three GPL distribution patterns, FG-X, UD, and FG-O, clearly shows that the FG-X configuration not only results in the highest critical thermal buckling load but also sustains a more stable postbuckling path with relatively lower deflection growth under increasing thermal load. This improved postbuckling performance can be attributed to the optimal reinforcement distribution in the FG-X scheme, which places GPLs near the shell surfaces where thermal bending effects are most significant; in contrast, the FG-O configuration exhibits the weakest postbuckling response. Fig. 3(b) demonstrates the effect of increasing the total GPL mass fraction on the postbuckling behavior. Higher mass fractions of GPL lead to both elevated critical buckling temperatures and stiffer postbuckling paths. This behavior reflects the enhancement of overall structural rigidity and thermal resistance due to the increased GPL reinforcement.

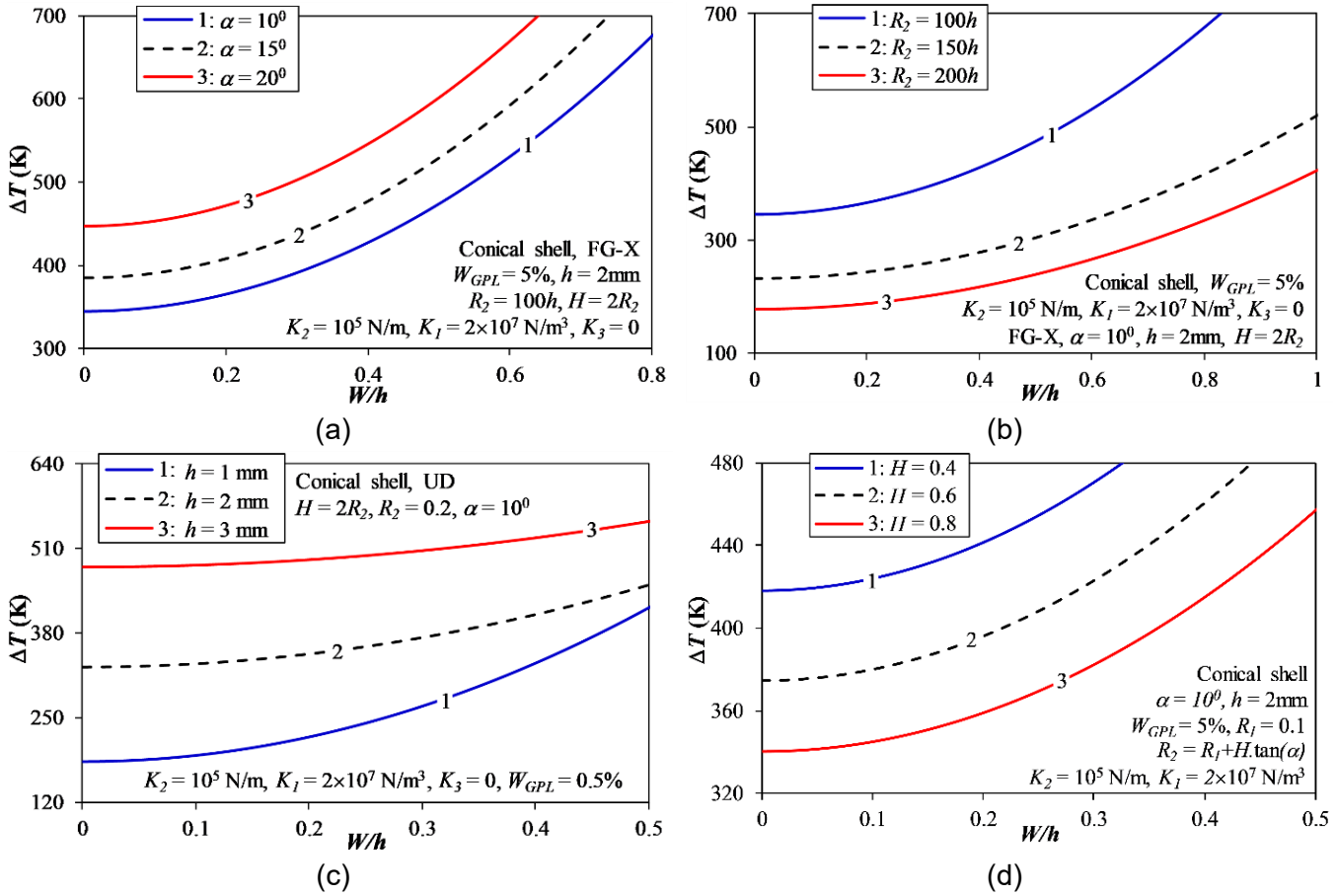

Fig. 4. Effects of geometrical parameters on the thermal postbuckling of FG-GPLRC conical shells

Fig. 4 provides a comprehensive visualization of how key geometrical parameters affect the thermal postbuckling behavior of FG-GPLRC conical shells. These parameters include the semi-top angle, the radius-to-thickness ratio R_2/h, and the shell length, all of which have a profound influence on the structural stiffness and deformation characteristics under thermal loading. In Fig. 4(a), the semi-top angle is varied. An increase in the semi-top angle results in an upward shift of both the critical buckling temperature and the postbuckling path. Larger semi-top angles correspond to more "open" conical geometries, which provide greater resistance to circumferential compressive stresses and thus enhance overall stability. Figs. 4(b) and 4(c) examine the effect of

increasing the R_2/h ratio and shell thickness h. As observed, higher R_2/h values or smaller shell thickness (i.e., thinner shells relative to their radius) lead to a significant drop in both the buckling load and the postbuckling stiffness.

Additionally, the postbuckling curves for higher R_2/h values or smaller h display shallow slopes, indicating increased sensitivity to further thermal loading and a higher risk of structural failure. Fig. 4(d) presents the influence of shell length. Longer shells tend to have weaker buckling resistance.

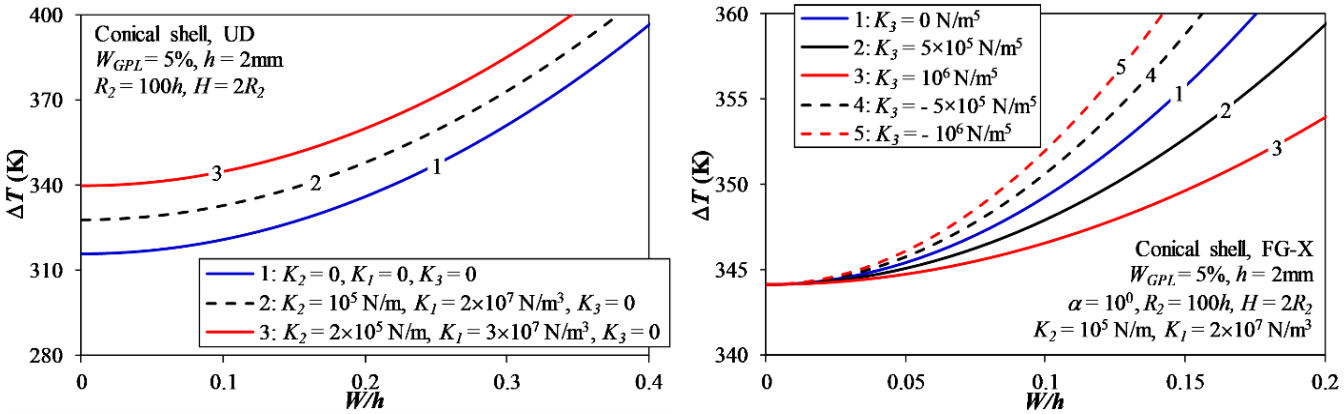

Fig. 5. Effects of foundation parameters on the thermal postbuckling of FG-GPLRC conical shells

Fig. 5 depicts the thermal postbuckling responses of FG-GPLRC conical shells with varying foundation stiffness parameters. The analyses focus on both the linear (Winkler and Pasternak) and nonlinear elastic foundation components to evaluate their contributions to the structural behavior under elevated thermal loading. In Fig. 5(a), the influence of increasing Winkler (K_1) and Pasternak (K_2) stiffness is clearly demonstrated. The presence of an elastic foundation substantially raises the critical thermal buckling temperature and enhances the postbuckling stiffness of the shell. This is due to the foundation providing additional restoring forces against lateral and shear deformations, effectively improving the shell's structural stiffness. Fig. 5(b) examines the contribution of nonlinear foundation stiffness (K_3). As the nonlinear stiffness component increases, a further improvement in the postbuckling response is observed. The nonlinear foundation introduces a displacement-dependent resistance, which becomes more pronounced at larger deformations, thus mitigating the postbuckling growth in deflection. Conversely, the thermal critical buckling load is not affected by the increase in the nonlinear foundation parameters. Finally, the bifurcation phenomenon is observed; conversely, the snap-through phenomenon is not obtained in all investigated examples.

5. Conclusions

An analytical approach has been developed to investigate the nonlinear thermal buckling and postbuckling behavior of FG-GPLRC conical shells resting on nonlinear elastic foundations. The theoretical formulation is based on Donnell shell theory combined with von Kármán geometric nonlinearity and employs the Ritz energy method to derive thermal load–deflection relationships. Key conclusions from the study are as follows:

1. Among the studied patterns, the FG-X distribution consistently provides superior thermal buckling resistance and enhanced postbuckling stiffness, owing to the distribution of GPLs near the shell surfaces where stress concentrations are highest.

2. Increasing the semi-top angle and shell

thickness significantly improves both the critical thermal buckling load and postbuckling performance, while higher radius-to-thickness ratios (R_2/h) and longer shell lengths reduce thermal stability due to increased slenderness and flexibility.

3. An increase in the total mass fraction of GPLs results in a substantial enhancement in thermal buckling resistance and structural stiffness. The effect is more pronounced for configurations with concentrated surface reinforcement.

4. Incorporating elastic foundations, both linear and nonlinear, raises the critical thermal buckling temperature and improves postbuckling behavior. In contrast, the nonlinear foundation stiffness, being associated with postbuckling deformation, has no effect on the critical buckling load but plays a crucial role in enhancing the postbuckling stability by providing displacement-dependent resistance.

Overall, this study highlights the importance of material property, structural geometry, and foundation modeling in enhancing the thermal stability of advanced composite shell structures. The proposed analytical framework can serve as a foundational tool for further parametric studies and design optimization in aerospace, mechanical, and marine engineering applications.

References

[1] S.Y. Lu, L.K. Chang. (1967). Thermal buckling of conical shells. *American Institute of Aeronautics and Astronautics*, 5(10), 1877-1882. https://doi.org/10.2514/3.4319

[2] L.K. Chang, S.Y. Lu. (1968). Nonlinear thermal elastic buckling of conical shells. *Nuclear Engineering and Design*, 7(2), 159-169. https://doi.org/10.1016/0029-5493(68)90057-5

[3] J. Tani. (1974). Dynamic instability of truncated conical shells under periodic axial load. *International Journal of Solids and Structures*, 10 (2), 169-176. https://doi.org/10.1016/0020-7683(74)90016-X

[4] J. Tani. (1976). Influence of deformations before instability on the parametric instability of conical shells under periodic pressure. *Journal of Sound and Vibration*, 45(2), 253-258. https://doi.org/10.1016/0022-460X(76)90600-3

[5] J. Tani. (1978). Influence of axisymmetric initial deflections on the thermal buckling of truncated conical shells. Nuclear *Engineering and Design*, 48(2-3), 393-403. https://doi.org/10.1016/0029-5493(78)90086-9

[6] J. Tani. (1984). Buckling of truncated conical shells under combined pressure and heating. *Journal of Thermal Stresses*, 7(3-4), 307-316. https://doi.org/10.1080/01495738408942214

[7] X.X. Hu, T. Sakiyama, H. Matsuda, C. Morita. (2002). Vibration analysis of twisted conical shells with tapered thickness. *International Journal of Engineering Science*, 40(14), 1579-1598. https://doi.org/10.1016/S0020-7225(02)00019-8

[8] X.X. Hu, T. Sakiyama, H. Matsuda, C. Morita. (2002). Vibration analysis of rotating twisted and open conical shells. *International Journal of Solids and Structures*, 39(25), 6121-6134. https://doi.org/10.1016/S0020-7683(02)00456-0

[9] C.S. Xu, Z.Q. Xia, C.Y. Chia. (1996). Non-linear theory and vibration analysis of laminated truncated, thick conical shells. *International Journal of Non-Linear Mechanics,* 31(2), 139-154. https://doi.org/10.1016/0020-7462(95)00051-8

[10] B.P. Patel, K.K. Shukla, Y. Nath. (2005). Thermal postbuckling analysis of laminated cross-ply truncated circular conical shells. *Composite Structures*, 71(1), 101-114. https://doi.org/10.1016/j.compstruct.2004.09.030

[11] K.Y. Lam, H. Li, T.Y. Ng, C.F. Chua. (2002). Generalized differential quadrature method for the free vibration of truncated conical panels. *Journal of Sound and Vibration*, 251(2), 329-348. https://doi.org/10.1006/jsvi.2001.3993

[12] X. Zhao, Q. Li, K.M. Liew, T.Y. Ng. (2006). The

element-free kp-Ritz method for vibration analysis of conical shell panels. *Journal of Sound and Vibration*, 295(3-5), 906-922. https://doi.org/10.1016/j.jsv.2006.01.045

[13] P. Paczos, J. Zielnica. (2008). Stability of orthotropic elastic–plastic open conical shells. *Thin-Walled* Structures, 46(5), 530-540. https://doi.org/10.1016/j.tws.2007.10.006

[14] H. Zhou, X. Shi, P. Zuo. (2026). Research on vibrational characteristics of joined spherical–conical–cylindrical shells with multiple annular plates. *Advances in Engineering Software*, 212, 104059. https://doi.org/10.1016/j.advengsoft.2025.104059

[15] A.H. Sofiyev. (2007). Thermoelastic stability of functionally graded truncated conical shells. *Composite Structures*, 77(1), 56-65. https://doi.org/10.1016/j.compstruct.2005.06.004

[16] A.H. Sofiyev. (2010). The buckling of FGM truncated conical shells subjected to combined axial tension and hydrostatic pressure. *Composite Structures*, 92(2), 488-498. https://doi.org/10.1016/j.compstruct.2009.08.033

[17] A.H. Sofiyev. (2011). Non-linear buckling behavior of FGM truncated conical shells subjected to axial load. *International Journal of Non-Linear Mechanics*, 46(5), 711-719. https://doi.org/10.1016/j.ijnonlinmec.2011.02.003

[18] A.H. Sofiyev. (2010). The buckling of FGM truncated conical shells subjected to axial compressive load and resting on Winkler–Pasternak foundations. *International Journal of Pressure Vessels and Piping*, 87(12), 753-761. https://doi.org/10.1016/j.ijpvp.2010.08.012

[19] R. Naj, M.S. Boroujerdy, M.R. Eslami. (2008). Thermal and mechanical instability of functionally graded truncated conical shells. *Thin-Walled Structures*, 46(1), 65-78. https://doi.org/10.1016/j.tws.2007.07.011

[20] D.H. Bich, N.T. Phuong, H.V. Tung. (2012). Buckling of functionally graded conical panels under mechanical loads. *Composite Structures*, 94(4), 1379-1384. https://doi.org/10.1016/j.compstruct.2011.11.029

[21] P. Malekzadeh, Y. Heydarpour. (2013). Free vibration analysis of rotating functionally graded truncated conical shells. *Composite Structures*, 97, 176-188. https://doi.org/10.1016/j.compstruct.2012.09.047

[22] O.E. Crenwelge, D. Muster. (1969). Free vibration of ring- and stringer-stiffened conical shells. *Journal of the Acoustical Society of America*, 46(1B), 176-185. https://doi.org/10.1121/1.1911667

[23] B.A.J. Mustaffa, R. Ali. (1987). Free vibration analysis of multisymmetric stiffened shells. *Computers & Structures*, 27(6), 803-810. https://doi.org/10.1016/0045-7949(87)90294-X

[24] F. Tornabene. (2009). Free vibration analysis of functionally graded conical, cylindrical and annular shell structures with a four-parameter power-law distribution. *Computer Methods in Applied Mechanics and Engineering*, 198(37-40), 2911-2935. https://doi.org/10.1016/j.cma.2009.04.011

[25] F. Tornabene, E. Viola, D.J. Inman. (2009). 2-D differential quadrature solution for vibration analysis of functionally graded conical, cylindrical and annular shell structures. *Journal of Sound and Vibration*, 328(3), 259-290. https://doi.org/10.1016/j.jsv.2009.07.031

[26] M. Mirzaei, Y. Kiani. (2015). Thermal buckling of temperature-dependent FG-CNT reinforced composite conical shells. *Aerospace Science and Technology*, 47, 42-53. https://doi.org/10.1016/j.ast.2015.09.011

[27] R. Ansari, J. Torabi. (2016). Numerical study on the buckling and vibration of functionally graded carbon nanotube-reinforced composite conical shells under axial loading. *Composite Part B: Engineering*, 95, 196-208. https://doi.org/10.1016/j.compositesb.2016.03.

080
[28] R. Ansari, J. Torabi, M.F. Shojaei, E. Hasrati. (2016). Buckling analysis of axially-loaded functionally graded carbon nanotube-reinforced composite conical panels using a novel numerical variational method. *Composite Structures*, 157, 398-411. https://doi.org/10.1016/j.compstruct.2016.08.028
[29] M. Hosseini, M. Talebitooti. (2018). Buckling analysis of moderately thick FG carbon nanotube-reinforced composite conical shells under axial compression by DQM. *Mechanics of Advanced Materials and Structures*, 25(8), 647-656. https://doi.org/10.1080/15376494.2017.1308597
[30] L.N. Quang, V.M. Duc, T.Q. Minh. (2024). Nonlinear buckling and postbuckling behaviors of porous FG-GPLRC cylindrical shells with stiffeners subjected to external pressure. *Journal of Science and Transport Technology*, 4(2), 24-36. https://doi.org/10.58845/jstt.utt.2024.en.4.2.24-36
[31] L.K. Hoa, V.T. Hung, P.H. Quan, V.H. Nam. (2021). Nonlinear buckling and postbuckling of spiral stiffened FG-GPLRC cylindrical shells subjected to torsional loads. *Journal of Science and Transport Technology*, 1(1), 24-33. https://doi.org/10.58845/jstt.utt.2021.en.1.1.24-33
[32] Y. Kiani. (2019). Buckling of functionally graded graphene-reinforced conical shells under external pressure in thermal environment. *Composites Part B: Engineering*, 156, 128-137. https://doi.org/10.1016/j.compositesb.2018.08.052
[33] R. Ansari, J. Torabi, E. Hasrati. (2020). Postbuckling analysis of axially-loaded functionally graded GPL-reinforced composite conical shells. *Thin-Walled Structures*, 148, 106594. https://doi.org/10.1016/j.tws.2019.106594
[34] R.B. Mahani, A. Eyvazian, F. Musharavati, T.A. Sebaey, P. Talebizadehsardari. (2020). Thermal buckling of laminated nanocomposite conical shell reinforced with graphene platelets. *Thin-Walled Structures*, 155, 106913. https://doi.org/10.1016/j.tws.2020.106913
[35] S. Yang, Z. Wang, Y. Hao, W. Zhang, Y. Niu, W. Ma. (2024). Nonlinear dynamic characteristics of smart FG-GPLRC sandwich varying-thickness truncated conical shell with internal resonance for first three-order modes. *Aerospace Science and Technology*, 155(2), 109672. https://doi.org/10.1016/j.ast.2024.109672
[36] Y. Heydarpour, P. Malekzadeh, R. Dimitri, F. Tornabene. (2020). Thermoelastic analysis of rotating multilayer FG-GPLRC truncated conical shells based on a coupled TDQM–NURBS scheme. *Composite Structures*, 235, 111707. https://doi.org/10.1016/j.compstruct.2019.111707
[37] R. Saboori, M. Ghadiri. (2024). Nonlinear forced vibration analysis of PFG-GPLRC conical shells under parametric excitation considering internal and external resonances. *Thin-Walled Structures*, 196, 111474. https://doi.org/10.1016/j.tws.2023.111474
[38] D.H. Duc, D.V. Thom, P.M. Phuc (2022). Buckling analysis of variable thickness cracked nanoplates considerting the flexoelectric effect. *Transport and Communications Science Journal*, 73 (5), 470-485. https://doi.org/10.47869/tcsj.73.5.3
[39] Y. Wang, R. Zeng, M. Safarpour. (2022). Vibration analysis of FG-GPLRC annular plate in a thermal environment. *Mechanics Based Design of Structures and Machines*, 50(1), 352-370. https://doi.org/10.1080/15397734.2020.1719508

Appendix

$$b_1 = \int_{x_0}^{x_0+L}\int_0^{2\pi}\left[\frac{\beta_2{}^2\left(\sin(n\theta)\right)^2\sin(\alpha)A_{22}}{x} + 4\frac{A_{12}m\pi\beta_1\left(\sin(n\theta)\right)^2\sin(\alpha)\beta_2}{L}\right]d\theta dx$$
$$+\int_{x_0}^{x_0+L}\int_0^{2\pi}\left[\frac{4m^2\pi^2\beta_1{}^2\left(\sin(n\theta)\right)^2 x\sin(\alpha)A_{11}}{L^2} + \frac{A_{66}\beta_2{}^2n^2\left(\cos(n\theta)\right)^2}{x\sin(\alpha)}\right]d\theta dx,$$

$$b_2 = \int_{x_0}^{x_0+L}\int_0^{2\pi}\beta_2\sin(n\theta)\left(\frac{\beta_4 n^2\sin(n\theta)}{x^2\left(\sin(\alpha)\right)^2} - \frac{m\pi\beta_3\sin(n\theta)}{xL}\right)\sin(\alpha)B_{22}d\theta dx$$
$$+\int_{x_0}^{x_0+L}\int_0^{2\pi}\left(\frac{m^2\pi^2\beta_4\beta_2}{L^2x} + \frac{2m\pi\beta_1}{L}\left(\frac{\beta_4 n^2}{x^2\left(\sin(\alpha)\right)^2} - \frac{m\pi\beta_3}{xL}\right)\right)x\sin(\alpha)B_{12}\left(\sin(n\theta)\right)^2 d\theta dx$$
$$+\int_{x_0}^{x_0+L}\int_0^{2\pi}\frac{2m^3\pi^3\beta_1\left(\sin(n\theta)\right)^2\beta_4 x\sin(\alpha)B_{11}}{L^3}d\theta dx + \int_{x_0}^{x_0+L}\int_0^{2\pi}\frac{\beta_4\left(\sin(n\theta)\right)^2\cot(\alpha)\beta_2\sin(\alpha)A_{22}}{x}d\theta dx$$
$$+\int_{x_0}^{x_0+L}\int_0^{2\pi}\frac{2m\pi\beta_1\left(\sin(n\theta)\right)^2\beta_4\cot(\alpha)\sin(\alpha)A_{12}}{L}d\theta dx + \int_{x_0}^{x_0+L}\int_0^{2\pi}\frac{2B_{66}\beta_2 n^2\left(\cos(n\theta)\right)^2\left(-\pi\beta_3 mx + L\beta_4\right)}{x^2\sin(\alpha)L}d\theta dx,$$

$$b_3 = \int_{x_0}^{x_0+L}\int_0^{2\pi}\frac{\beta_4{}^3n^3\cos(2n\theta)\left(\cos(n\theta)\right)^2A_{22}}{x^2\left(\sin(\alpha)\right)^2}d\theta dx + \int_{x_0}^{x_0+L}\int_0^{2\pi}\frac{m^2\pi^2\beta_3{}^2\left(\sin(n\theta)\right)^2\beta_4 n\cos(2n\theta)A_{12}}{L^2}d\theta dx$$
$$-\int_{x_0}^{x_0+L}\int_0^{2\pi}\frac{2A_{66}m\pi\beta_3\beta_4 n\left(L\beta_4 - \pi mx\beta_3\right)\left(\cos(n\theta)\right)^2\left(\sin(n\theta)\right)^2}{xL^2}d\theta dx,$$

$$b_4 = \int_{x_0}^{x_0+L}\int_0^{2\pi}\frac{4A_{22}\beta_4{}^2n^2\left(\cos(2n\theta)\right)^2}{x\sin(\alpha)} + \frac{A_{66}\left(\sin(2n\theta)\right)^2\left(-\pi\beta_3 mx + L\beta_4\right)^2\sin(\alpha)}{xL^2}d\theta dx,$$

$$b_5 = \int_{x_0}^{x_0+L}\int_0^{2\pi}\frac{\beta_4{}^4n^4\left(\cos(n\theta)\right)^4A_{22}}{2x^3\left(\sin(\alpha)\right)^3} + \frac{m^2\pi^2\beta_3{}^2\left(\sin(n\theta)\right)^2\beta_4{}^2n^2\left(\cos(n\theta)\right)^2A_{12}}{L^2x\sin(\alpha)}d\theta dx$$
$$+\int_{x_0}^{x_0+L}\int_0^{2\pi}\frac{m^4\pi^4\beta_3{}^4\left(\sin(n\theta)\right)^4 x\sin(\alpha)A_{11}}{2L^4}d\theta dx - \int_{x_0}^{x_0+L}\int_0^{2\pi}K_3\beta_4{}^4\left(\sin(n\theta)\right)^4 x\sin(\alpha)d\theta dx$$
$$+\int_{x_0}^{x_0+L}\int_0^{2\pi}\frac{2A_{66}m^2\pi^2\beta_3{}^2\left(\sin(n\theta)\right)^2\beta_4{}^2n^2\left(\cos(n\theta)\right)^2}{L^2x\sin(\alpha)}d\theta dx,$$

$$b_6 = \int_{x_0}^{x_0+L}\int_0^{2\pi}\frac{2\beta_4{}^3n^3\cos(2n\theta)\left(\cos(n\theta)\right)^2A_{22}}{x^2\left(\sin(\alpha)\right)^2} + \frac{2m^2\pi^2\beta_3{}^2\left(\sin(n\theta)\right)^2\beta_4 n\cos(2n\theta)A_{12}}{L^2}d\theta dx$$
$$-\int_{x_0}^{x_0+L}\int_0^{2\pi}\frac{4A_{66}m\pi\beta_3\left(\sin(n\theta)\right)^2\beta_4 n\left(\cos(n\theta)\right)^2\left(L\beta_4 - \pi\beta_3 mx\right)}{xL^2}d\theta dx,$$

$$b_7 = \int_{x_0}^{x_0+L}\int_0^{2\pi}\left(-\Phi_{1x}m^2\pi^2\beta_3{}^2\left(\sin(n\theta)\right)^2/L^2 - \Phi_{1\theta}\beta_4{}^2n^2\left(\cos(n\theta)\right)^2/x^2\left(\sin(\alpha)\right)^2\right)x\sin(\alpha)d\theta dx,$$

$$b_8 = \int_{x_0}^{x_0+L}\int_0^{2\pi} \frac{\beta_2 B_{22}\left(\sin(n\theta)\right)^2\left(-\pi\left(\sin(\alpha)\right)^2\beta_3 mx + L\beta_4 n^2\right)}{\sin(\alpha)x^2 L}d\theta dx +$$

$$+ \int_{x_0}^{x_0+L}\int_0^{2\pi}\left(\frac{m^2\pi^2\beta_4\beta_2}{L^2 x} + \frac{2m\pi\beta_1}{L}\left(\frac{\beta_4 n^2}{x^2\left(\sin(\alpha)\right)^2} - \frac{m\pi\beta_3}{xL}\right)\right)x\sin(\alpha)B_{12}\left(\sin(n\theta)\right)^2 d\theta dx +$$

$$+ \int_{x_0}^{x_0+L}\int_0^{2\pi}\frac{2m^3\pi^3\beta_1\left(\sin(n\theta)\right)^2\beta_4 x\sin(\alpha)B_{11}}{L^3}d\theta dx + \int_{x_0}^{x_0+L}\int_0^{2\pi}\frac{\beta_4\left(\sin(n\theta)\right)^2\cot(\alpha)\beta_2\sin(\alpha)A_{22}}{x}d\theta dx$$

$$+ \int_{x_0}^{x_0+L}\int_0^{2\pi}\frac{2m\pi\beta_1\left(\sin(n\theta)\right)^2\beta_4\cot(\alpha)\sin(\alpha)A_{12}}{L}d\theta dx + \int_{x_0}^{x_0+L}\int_0^{2\pi}\frac{2B_{66}\beta_2 n^2\left(\cos(n\theta)\right)^2\left(L\beta_4 - \pi\beta_3 mx\right)}{\sin(\alpha)x^2 L}d\theta dx,$$

$$b_9 = \int_{x_0}^{x_0+L}\int_0^{2\pi}\left[\frac{D_{22}\left(\sin(n\theta)\right)^2\left(L\beta_4 n^2 - \pi\left(\sin(\alpha)\right)^2\beta_3 mx\right)^2}{x^3\left(\sin(\alpha)\right)^3 L^2} - \beta_4^2\left(\sin(n\theta)\right)^2 x\sin(\alpha)K_1\right]d\theta dx$$

$$+ \int_{x_0}^{x_0+L}\int_0^{2\pi}\frac{2m^2\pi^2\beta_4 D_{12}\left(\sin(n\theta)\right)^2\left(-\pi\left(\sin(\alpha)\right)^2\beta_3 mx + L\beta_4 n^2\right)}{L^3 x\sin(\alpha)}d\theta dx$$

$$+ \int_{x_0}^{x_0+L}\int_0^{2\pi}2\beta_4\cot(\alpha)\left(\frac{\beta_4 n^2}{x^2\left(\sin(\alpha)\right)^2} - \frac{m\pi\beta_3}{xL}\right)\sin(\alpha)B_{22}\left(\sin(n\theta)\right)^2 d\theta dx$$

$$+ \int_{x_0}^{x_0+L}\int_0^{2\pi}\left[\frac{m^4\pi^4\beta_4^2\left(\sin(n\theta)\right)^2 x\sin(\alpha)D_{11}}{L^4} + \frac{2m^2\pi^2\beta_4^2\left(\sin(n\theta)\right)^2\cot(\alpha)\sin(\alpha)B_{12}}{L^2}\right]d\theta dx$$

$$+ \int_{x_0}^{x_0+L}\int_0^{2\pi}\left[\frac{\beta_4^2\left(\sin(n\theta)\right)^2\left(\cot(\alpha)\right)^2\sin(\alpha)A_{22}}{x} + 4\frac{D_{66}\left(\cos(n\theta)\right)^2 n^2\left(-\pi\beta_3 mx + L\beta_4\right)^2}{x^3\sin(\alpha)L^2}\right]d\theta dx$$

$$- \int_{x_0}^{x_0+L}\int_0^{2\pi}K_2\left(-\frac{m^2\pi^2\beta_4}{L^2} + \frac{m\pi\beta_3}{xL} - \frac{\beta_4 n^2}{x^2\left(\sin(\alpha)\right)^2}\right)\beta_4 x\sin(\alpha)\left(\sin(n\theta)\right)^2 d\theta dx,$$

where

$$\beta_1 = \cos\left(2\frac{m\pi(x-x_0)}{L}\right), \beta_2 = \sin\left(2\frac{m\pi(x-x_0)}{L}\right), \beta_3 = \cos\left(\frac{m\pi(x-x_0)}{L}\right), \beta_4 = \sin\left(\frac{m\pi(x-x_0)}{L}\right)$$